ACS Sustainable Chemistry & Engineering

pubs.acs.org/journal/ascecg

Research Article

Metabolic Engineering of *Escherichia coli* for *De Novo* Biosynthesis of the Platform Chemical Pelletierine

Wei Li, Peng Zhao, Ying Li, Shimin Wu, and Pingfang Tian*

Cite This: *ACS Sustainable Chem. Eng.* 2025, 13, 778−790

Read Online

ACCESS | Metrics & More | Article Recommendations | Supporting Information

ABSTRACT: Pelletierine is a versatile plant alkaloid having a C5N−C3 structure from which numerous chemicals can be derived. One notable derivative is huperzine A (HupA) which may alleviate the symptoms of Alzheimer's disease. Currently, industrial production of pelletierine relies primarily on chemical synthesis and plant extraction. However, chemical synthesis leads to analogues that complicate product separation, and plant extraction is constrained by limited resources. Herein, we report that pelletierine can be produced by recombinant *Escherichia coli* in which the engineered pelletierine biosynthesis pathway comprises four modules involving seven key genes native to *E. coli*, three genes from other bacteria, and three genes from plants. To overproduce pelletierine, the intrinsic L-lysine biosynthesis pathway in *E. coli* was simplified, and a clustered regularly interspaced short palindromic repeats (CRISPR) interference (CRISPRi) system was engineered to minimize the byproducts. Moreover, the transporter MatC was overexpressed to enhance the intracellular concentration of 3-oxoglutaryl ketide, which is another precursor of pelletierine. Based on the aforementioned manipulations, the resulting recombinant *E. coli* harboring the pelletierine biosynthesis pathway and CRISPRi system produced 3.40 and 8.23 mg/L pelletierine in a shake-flask and a 5 L bioreactor, respectively. This is the first report of microbial production of pelletierine, which represents a sustainable route to produce the precursor of HupA and beyond.

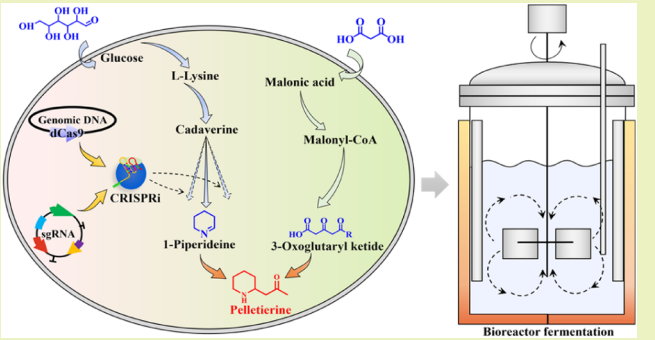

KEYWORDS: *huperzine A, pelletierine, Alzheimer's disease, Escherichia coli, metabolic engineering*

INTRODUCTION

The past decade has witnessed dementia becoming an ever-growing threat to human health.[1] In 2019, approximately 55 million people worldwide suffered from dementia,[2] and this situation is getting worse. According to the information from the World Health Organization, the number of dementia patients will reach approximately 139 million by 2050.[2] Of factors giving rise to dementia, Alzheimer's disease (AD) is a major reason in 60−80% patients,[3] as AD is a devastating neurodegenerative disease manifesting symptoms of memory loss, cognitive deficit, and behavioral abnormality.[1,4] By 2050, the annual cost of treating AD will reach $1 trillion.[5] Namely, by then, the global healthcare system will be under tremendous pressure. To cope with this crisis, great efforts have been made, including the development of early diagnosis techniques such as fluorodeoxyglucose positron emission tomography[6] and drugs such as monoclonal antibodies— aducanumab—to relieve symptoms. Despite these achievements, the treatment of AD remains challenging. Huperzine A (HupA) is an attractive Lycopodium alkaloid, as it can alleviate AD[7−9] by reversibly inhibiting acetylcholinesterase (AChE).[7] Compared to other medicines such as tacrine and galanthamine[7] for treating AD, HupA shows merits of long effect, high safety, and remarkable stability,[7,10] and it is thus a promising medicine to combat AD.[8,11] Currently, HupA has been approved as a therapeutic drug for AD in China, and it has been chosen as a dietary supplement in USA.[9]

As a crucial precursor of HupA,[8,11] pelletierine is a 2-acetonyl-substituted piperidine with a simple chemical structure.[12] Although pelletierine was initially isolated from pomegranate (*Punica granatum* L.) in 1878,[12−14] its precise structure was not deciphered until the first synthesis in 1961 because it usually coexists with isopelletierine.[12−14] Pelletierine is a versatile platform chemical because it has a C5N−C3 structure from which a panel of chemicals such as *N*-methylpelletierine, sedridine, anaferine, and pseudopelletierine can be derived[15,16] (Figure 1a). The pelletierine-derived pseudepelletierine can be further converted into cyclo-octatetraene.[17,18] Isotope labeling studies revealed that pellet-

Received: July 20, 2024
Revised: December 8, 2024
Accepted: December 9, 2024
Published: January 9, 2025

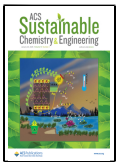

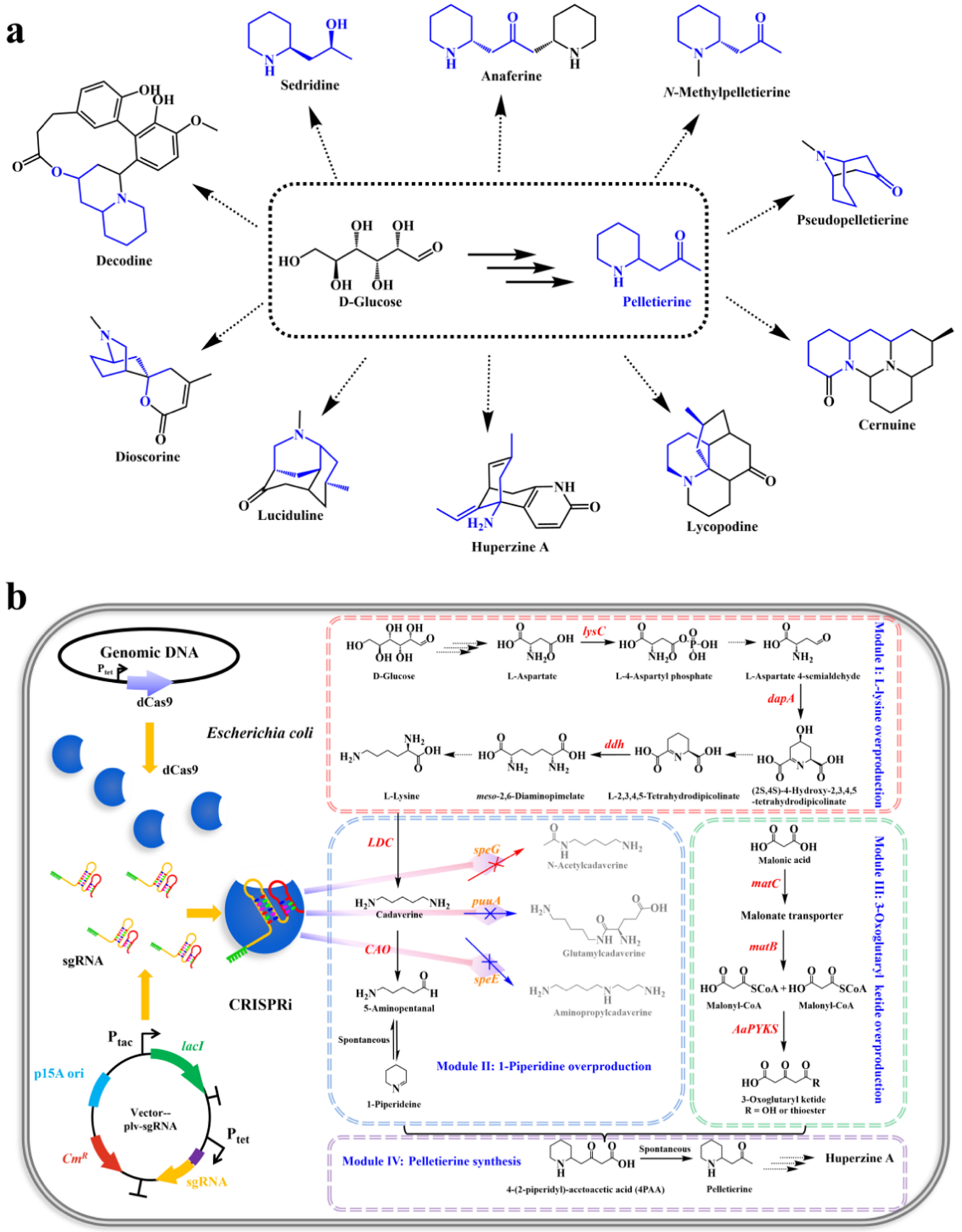

Figure 1. Derivatives and biosynthesis pathway of pelletierine. (a) Representative alkaloids derived from pelletierine. (b) Schematic diagram of engineering the pelletierine biosynthesis pathway and CRISPRi system in *E. coli*. The reconstituted pelletierine biosynthesis pathway comprises four modules: the L-lysine module for glucose conversion to L-lysine, Δ^1-piperideine module for L-lysine conversion to Δ^1-piperideine, 3-oxoglutaryl

https://doi.org/10.1021/acssuschemeng.4c05975
ACS Sustainable Chem. Eng. 2025, 13, 778−790

Figure 1. continued

ketide module for malonic acid conversion to 3-oxoglutaryl ketide, and pelletierine module for 4-(2-piperidyl)-acetoacetic acid conversion to pelletierine. In the Δ^1-piperideine module, the *dCas9* expression cassette was inserted into the *speG* gene in the *E. coli* genome, and two sgRNAs were designed to repress competing pathways and therefore improve 5-aminopentanal production. The overexpressed genes are highlighted in red. Knockdown and knockout are shown as blue cross and red cross, respectively. Abbreviations: *lysC*, aspartate kinase; *dapA*, 4-hydroxy-tetrahydrodipicolinate synthase; *ddh*, *meso*-diaminopimelate dehydrogenase; *LDC*, lysine decarboxylase; *CAO*, copper amine oxidase; *puuA*, γ-glutamylputrescine synthase; *speE*, spermidine synthase; *speG*, diamine *N*-acetyltransferase; *matC*, putative malonate carrier protein; *matB*, malonyl-CoA synthetase; *AaPYKS*, pyrrolidine ketide synthases.

ierine is an obligatory intermediate in the biosynthesis of Lycopodium alkaloids such as luciduline, cernuine, lycodine-obscurine, HupA, and lycopodine-type[15,16] (Figure 1a). Apart from aforementioned chemicals, more complex chemicals such as decodine which is a Lythraceae alkaloid can also be derived from pelletierine.[16] Critically, most of the above mentioned derivatives have shown potential therapeutic applications. For instance, pelletierine and *N*-methylpelletierine could be exploited as antihelminthic drugs,[14] and sedridine could be harnessed for alleviating asthma, bronchitis, and pneumonia owing to its versatile biological activities.[19,20] As a C2-symmetrical bis-piperidine alkaloid, anaferine shows potential to alleviate neurodegenerative diseases due to nAChR agonist activity and inhibition against GluN2B-containing NMDA receptors.[21] Extant strategies to source pelletierine mainly include plant extraction and chemical synthesis. While plant extraction relies on a time-consuming agricultural process, chemical synthesis requires expensive reagents, catalysts, and precursors,[22] which are reminiscent of high production cost. In particular, chemical synthesis leads to analogues that extremely complicate downstream separation. In contrast, biomanufacturing seems to be more sustainable in this regard.[23]

Previously, pelletierine was biosynthesized from L-lysine, which was subsequently used as a feedstock for chemical synthesis of HupA.[11] Biosynthesis of HupA requires multistep catalysis, and it is challenging to express complex enzymes such as P450.[8,11] So far, most putative enzymes for biosynthesis of pelletierine and HupA have been validated.[8,11,15] Biosynthesis of pelletierine starts from L-lysine, which is decarboxylated and oxidized to form Δ^1-piperideine. Next, Δ^1-piperideine is coupled with 3-oxoglutaryl ketide to form 4-(2-piperidyl)-acetoacetic acid (4PAA) or 4PAA-CoA, which subsequently undergoes spontaneous decarboxylation to form pelletierine.[11,15] To date, several key enzymes participating in the biosynthesis of L-lysine, Δ^1-piperideine, and 3-oxoglutaryl ketide have been identified, including aspartate kinase (LysC),[24,25] 4-hydroxy-tetrahydrodipicolinate synthase (DapA),[24,26] *meso*-diaminopimelate dehydrogenase (DapDH),[27,28] lysine decarboxylase (LDC),[11,15] copper amine oxidase (CAO),[11,15] putative malonate carrier protein (MatC),[29,30] malonyl-CoA synthetase (MatB),[29,30] and polyketide synthase III (PKS III)[31−33] (Figure 1b and Table S3).

In view of the aforementioned information, we conjectured that bioproduction of pelletierine might be feasible due to available enzymes and powerful regulation tools such as clustered regularly interspaced short palindromic repeats (CRISPR) interference (CRISPRi) for diminishing byproducts (Figure 1b). To test this prediction, we constructed four functional modules: the L-lysine module for glucose conversion to L-lysine, Δ^1-piperideine module for L-lysine conversion to Δ^1-piperideine, 3-oxoglutaryl ketide module for malonic acid conversion to 3-oxoglutaryl ketide, and pelletierine module for 4-(2-piperidyl)-acetoacetic acid conversion to pelletierine. To minimize byproducts, we engineered a CRISPRi system consisting of two parts: a *tet* promoter-driven *dCas9* expression cassette inserted into the *E. coli* genome and two sgRNAs tailored to repress γ-glutamylputrescine synthase (*puuA*) and spermidine synthase (*speE*), which catalyze the formation of two byproducts glutamyl cadaverine and aminopropyl cadaverine, respectively (Figure 1b). By optimizing the addition time of inducers and the concentrations of substrates, the engineered CRISPRi system was expected to minimize byproducts and accordingly maximize pelletierine. Transcription analysis of the genes governing byproducts aimed to screen best-performing sgRNAs. Shake-flask fermentation of recombinant *E. coli* aimed to clarify the influence of the CRISPRi system on pelletierine production. Lastly, bioreactor cultivation of this strain aimed to investigate its performance in large-scale fermentation.

MATERIALS AND METHODS

Strains and Medium. *E. coli* TOP10 was used for plasmid construction. *E. coli* BL21(DE3) was used as the initial strain for pelletierine production. *E. coli* TOP10 was grown in Luria−Bertani (LB) medium containing the following ingredients per liter: tryptone (10 g), NaCl (10 g), and yeast extract (5 g). *E. coli* BL21(DE3) was grown in a medium containing the following ingredients per liter: $MgSO_4·7H_2O$, 0.5 g; $CaCO_3$, 0.01 g; MOPS, 2 g; Na_2HPO_4, 6 g; KH_2PO_4, 3 g; NaCl, 0.5 g; NH_4Cl, 2 g; $(NH_4)_2SO_4$, 1 g; yeast extract, 5 g; and $C_6H_{12}O_6$, 20 g. Chemicals including L-lysine, pyridoxal-5′-phosphate (PLP) cofactor,[34] 2,4,5-trihydroxyphenylalanine quinone (TPQ),[35] malonic acid, 3-oxoglutaryl ketide, Δ^1-piperideine, and pelletierine were purchased from Shanghai Bide Pharmaceutical Technology Co., Ltd. Restriction enzymes, Q5 DNA polymerase, and T4 DNA ligase were purchased from Thermo Fisher Scientific (Beijing, China). pKD13 and pCP20 plasmids were purchased from NovoPro Bioscience, Inc. Primer synthesis and DNA sequencing (Table S2) were performed by Biomed Co., Ltd. Other chemicals for screening strains and gel electrophoresis were purchased from Sigma-Aldrich (Shanghai, China).

Plasmid Construction. Oligonucleotides were synthesized by Sangon Biotech (Shanghai, China). All DNA manipulations followed the standard molecular cloning procedures or manufacturers' instructions. The plasmid pET28a was used to construct the biosynthesis pathways of L-lysine and Δ^1-piperideine. The vector plv[36] carrying the *tac* promoter and p15A replicon was used to construct the 3-oxoglutaryl ketide pathway and the CRISPRi system (Table S1).

Construction of the CRISPRi System. *sgRNA Cassette Construction.* To modulate the cadaverine pathway for overproducing 5-aminopentanal, two genes *puuA* and *speE* in competing pathways, which encode γ-glutamylputrescine synthase and spermidine synthase, respectively, were chosen as the targets of the CRISPRi system. The sgRNA cassette was derived from the plasmid plv-sgRNA, which contains an sgRNA chimera driven by a TetR-inducible *tet* promoter (P_{tet}). The *Bsp*QI site in the vector plv-sgRNA was used for sgRNA insertion without leaving a scar. For the construction of different sgRNA cassettes, only the sgRNA sequence in the vector plv-sgRNA was replaced. To ensure efficient inhibition, three candidate sgRNAs targeting different regions of byproduct

https://doi.org/10.1021/acssuschemeng.4c05975
ACS Sustainable Chem. Eng. 2025, 13, 778−790

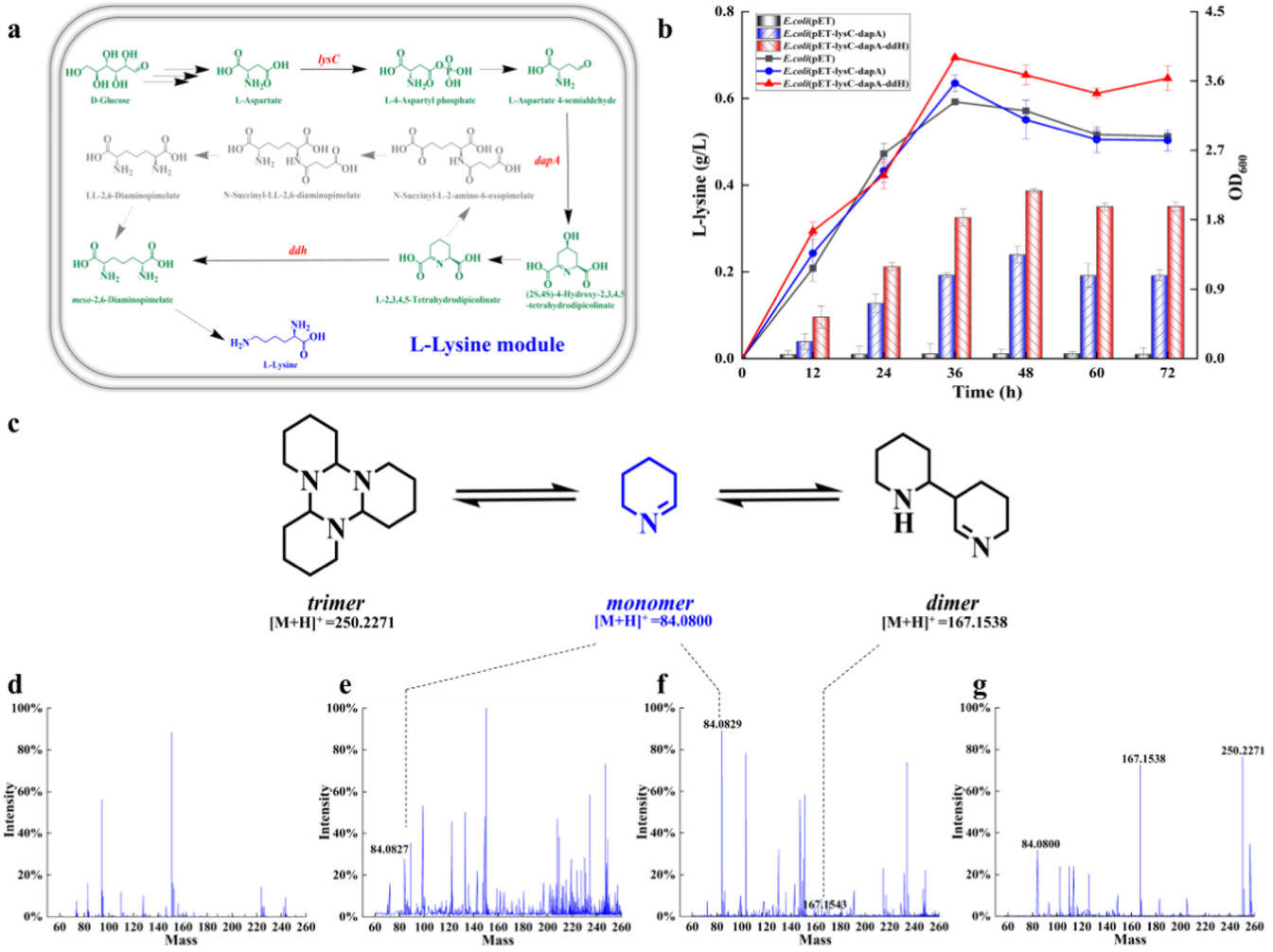

Figure 2. Shortened L-lysine biosynthesis pathway in *E. coli* for producing L-lysine and Δ^1-piperideine from glucose. (a) Simplified L-lysine biosynthesis pathway using the *Corynebacterium glutamicum* DapDH enzyme (encoded by *ddh*) to replace four enzymes native to *E. coli* for one-step conversion of tetrahydrodipicolinate (L-2,3,4,5-tetrahydrodipicolinate) to *meso*-diaminopimelate (*meso*-2,6-diaminopimelate). (b) Time courses of the recombinant *E. coli* strains overexpressing the key genes for L-lysine synthesis. (c) Δ^1-piperideine is in equilibrium with its dimer and trimer. (d) LC−MS analysis of the fermentation broth of the strain *E. coli*(pET) devoid of Δ^1-piperideine. (e) LC−MS analysis of Δ^1-piperideine ($[M + H]^+=m/z$ 84.0827) produced by the strain *E. coli*(pET-lysC-dapA-ddh-CAO-LDC). (f) LC−MS analysis of Δ^1-piperideine ($[M + H]^+=m/z$ 84.0829) and its dimer ($[M + H]^+=m/z$ 167.1543) produced by *E. coli*Δ*speG*(pET-lysC-dapA-ddh-CAO-LDC). (g) LC−MS analysis of the standard Δ^1-piperideine ($[M + H]^+=m/z$ 84.0800) containing its dimer ($[M + H]^+=m/z$ 167.1538) and trimer ($[M + H]^+=m/z$ 250.2271). *E. coli*(pET), recombinant *E. coli* strain harboring the vector pET; *E. coli*(pET-lysC-dapA), recombinant *E. coli* strain harboring the vector pET-lysC-dapA; *E. coli*(pET-lysC-dapA-ddh), recombinant *E. coli* strain harboring the vector pET-lysC-dapA-ddh; *E. coli*(pET-lysC-dapA-ddh-CAO-LDC), recombinant *E. coli* strain harboring the vector pET-lysC-dapA-ddh-CAO-LDC; *E. coli*Δ*speG*(pET-lysC-dapA-ddh-CAO-LDC), recombinant *E. coli*Δ*speG* strain harboring the vector pET-lysC-dapA-ddh-CAO-LDC. The results represent the mean ± s.d. of triplicates (n = 3).

synthesis genes were chemically synthesized (Figure 5a), and the resulting sgRNA vectors were named after respective genes (Figure 5a).

dCas9 Expression Cassette Construction. Considering that the CRISPRi system can simultaneously knock down multiple genes due to an array of guide RNA,[37,38] it was thus engineered in *E. coli* to minimize cadaverine-derived byproducts and accordingly maximize 5-aminopentanal.[39] The CRISPRi system was engineered by Lambda Red homologous recombination. Briefly, the upstream and downstream homologous arms of diamine *N*-acetyltransferase coding gene *speG* (int) were cloned from the *E. coli* genome. The *dCas9* expression cassette P_{tet}-*dCas9* was cloned from the plasmid plv-*dCas9*-sgRNA, and the FRT-Kan-FRT (FKF) resistance gene was cloned from the plasmid pKD13. PCR amplification and subsequent Gibson assembly of the aforementioned four fragments resulted in a vector named T-speG(int)-*dCas9*-FKF, and this vector was then transformed into competent *E. coli* and confirmed by colony PCR and DNA sequencing.

Integration of the dCas9 Expression Cassette into the E. coli Genome. To minimize plasmid burden and stabilize the CRISPRi system, the P_{tet}-*dCas9* cassette was integrated into the *E. coli* genome by Lambda Red homologous recombination. Briefly, the fragment speG(int)-*dCas9*-FKF was cloned from the vector T-speG(int)-d*Cas9*-FKF and transformed into *E. coli*. Next, this fragment underwent a recombination with the homologous region in genome due to the presence of *β*, Exo, and Gam proteins.[40] Lastly, the plasmid pCP20 was transformed into recombinant *E. coli*-*dCas9*-FKF to eliminate the FKF fragment. Afterward, a single colony was moved to the LB plate. The strains able to survive in the LB plate devoid of chloramphenicol but unable to survive in the LB chloramphenicol plate were subjected to PCR amplification. To confirm the *dCas9* cassette integration into the *E. coli* genome, the *dCas9* fragment was amplified by PCR using the primers flanking the *speG* gene.

PCR Analysis of CRISPRi System-Targeted Genes. To screen sgRNAs efficient for repressing gene expression, reverse transcription and quantitative PCR (RT-qPCR) were performed. Briefly, the

https://doi.org/10.1021/acssuschemeng.4c05975
ACS Sustainable Chem. Eng. 2025, 13, 778−790

recombinant strains were grown in a fermentation medium containing an antibiotic and an inducer. The recombinant strain grown in the same medium but without an inducer was used as the control. Cells were harvested by centrifugation at 12,000 rpm for 5 min when the OD_{600} of fermentation broth reached 0.3. Total RNA was extracted using the TRIzol reagent. DNA contamination was eliminated by RNase-free DNase I. cDNAs were synthesized by reverse transcription of RNA samples. RT-qPCR was performed by an Applied Biosystems 7900HT Fast Real-Time PCR System (Thermo Fisher) with SYBR Green. The glyceraldehyde-3-phosphate dehydrogenase (GAPDH) coding gene was used as the internal control to determine the relative expression levels of the genes. Statistic analysis was conducted using the $2^{-\Delta\Delta Ct}$ strategy.

Shake-Flask and Bioreactor Cultivation. *E. coli* strains were individually grown in 250 mL shake-flasks, each containing 100 mL of fermentation medium and appropriate antibiotics, at 37 °C and 180 rpm. After 3 h of cultivation, IPTG at a final concentration of 0.5 mM or anhydrotetracycline (ATC) at a final concentration of 2 μM[41] was added into M9 medium to trigger gene expression at 30 °C. Prior to fed-batch cultivation, the strain was precultured in 100 mL LB medium at 37 °C. Subsequently, the strain was moved to a 5 L bioreactor (Baoxing, China) containing 1.5 L fermentation medium, antibiotics (kanamycin and chloramphenicol), cofactors (PLP and TPQ), substrates (glucose and malonic acid), and inducers (IPTG and ATC) for pelletierine production. Air was supplied at 1.5 vvm. The agitation speed was 400 rpm. The temperature was 30 °C, and the pH value was maintained at 7.0 by adding 5 M NaOH or 1 M HCL. Samples were taken out every 3 h to examine the biomass, residual glucose, and malonic acid.

Analytical Methods. The cell density was measured with an automatic microplate reader at 600 nm with 200 μL of fermentation broth. The cell growth was calculated using the following equation: $\mu = (\ln X_2 - \ln X_1)/(t_2 - t_1)$, where X_1 and X_2 indicate the OD_{600} values at culture times t_1 and t_2, respectively. To examine the glucose concentration, cells were harvested by centrifugation at 12,000 rpm for 10 min. Subsequently, the supernatant was filtered through a 0.2 μm syringe filter and then analyzed using an SBA-40E immobilized enzyme biosensor (Shandong, China).[42] L-Lysine was determined with a high-performance liquid chromatography (HPLC) system (Shimadzu, Kyoto, Japan) equipped with a C18 column and an SPD-20A UV detector at 254 nm. The column temperature was 40 °C, and the mobile phase was methanol and water (containing 0.1% formic acid) for gradient elution at 1 mL/min upon precolumn derivatization with phenyl isothiocyanate (PITC). Malonic acid was analyzed by HPLC at 235 nm using an ion-exchange column (Aminex HPX-87H, 7.8 × 300 mm^2, BioRad). The mobile phase was 5 mM H_2SO_4 at 0.6 mL/min flow rate. Δ^1-piperideine and pelletierine were analyzed by liquid chromatography−mass spectrometry (LC−MS). The electrospray ionization mass spectrometry (ESI-MS) spectrum was obtained using a Waters system. Gradient elution was conducted in a Waters ACQUITY UPLC BEH Amide column (1.7 μm, 2.1 × 100 mm^2) using the mobile phase of solvent A (water + 0.1% formic acid) plus solvent B (acetonitrile) at 0.3 mL/min for 12 min until termination. Finally, the peak area was calculated by the external standard method.

RESULTS

Performance of the Shortened L-Lysine Module. Glucose-based biosynthesis of L-lysine in *E. coli* involves the glycolysis pathway, pentose phosphate pathway, tricarboxylic acid (TCA) cycle, and diaminopimelic acid pathway.[26,27] To overproduce L-lysine, LysC (EC 2.7.2.4, encoded by *lysC*) was coexpressed with DapA (EC 4.3.3.7, encoded by *dapA*), and the corresponding recombinant strain *E. coli*(pET-lysC-dapA) demonstrated a maximal OD_{600} of 3.57 at 36 h. HPLC analysis revealed 0.24 g/L L-lysine production at 48 h, which was much higher than that produced by the control strain *E. coli*(pET) (Figure 2b). Interestingly, after 48 h, the L-lysine level showed a slight decline, which was possibly ascribed to halted cell growth. Nevertheless, the overexpression of LysC and DapA benefited L-lysine biosynthesis.

To further improve L-lysine production, we attempted to shorten its biosynthetic pathway. In wild-type *E. coli*, L-lysine biosynthesis is largely influenced by the conversion of tetrahydrodipicolinate (L-2,3,4,5-tetrahydrodipicolinate) to *meso*-diaminopimelate (*meso*-2,6-diaminopimelate), which is undertaken by four successive enzymatic reactions (Figure 2a). To replace the four enzymes, the *meso*-diaminopimelate dehydrogenase (DapDH, EC 1.4.1.16, encoded by *ddh*) from *C. glutamicum* was recruited for the one-step conversion of tetrahydrodipicolinate to *meso*-diaminopimelate (Figure 2a). With this in mind, DapDH would be coexpressed with aforementioned enzymes LysC and DapA. Briefly, the vector pET-lysC-dapA-ddh coexpressing *lysC*, *dapA*, and *ddh* genes was constructed and transformed into *E. coli*. As expected, the resulting recombinant strain named *E. coli*(pET-lysC-dapA-ddh) not only grew faster but also produced more L-lysine compared to the strain *E. coli*(pET-lysC-dapA) devoid of the *ddh* gene, indicating the coupling between lysine formation and cell growth (Figure 2b). Notably, the strain *E. coli*(pET-lysC-dapA-ddh) showed a maximal OD_{600} of 3.90 at 36 h and synthesized 0.38 g/L L-lysine at 48 h. By contrast, at the same two time points 36 and 48 h, the strain *E. coli*(pET-lysC-dapA) lacking the *ddh* gene showed lower OD_{600} and less L-lysine formation. These results suggested that the enzyme DapDH from *C. glutamicum* outperformed the four enzymes native to *E. coli* in the biosynthesis of L-lysine because it enabled one-step conversion of tetrahydrodipicolinate to *meso*-diaminopimelate. This finding was consistent with the previous study.[27] Overall, the simplification of the L-lysine pathway benefited L-lysine biosynthesis.

Performance of the Δ^1-Piperideine Module. While sufficient L-lysine is crucial for the high-level production of Δ^1-piperideine, Δ^1-piperideine seems to be an indispensable feedstock for pelletierine biosynthesis. It has been reported that pelletierine can be produced by Mannich-like condensation of Δ^1-piperideine and 3-oxoglutaryl ketide, followed by spontaneous decarboxylation.[15] Δ^1-piperideine is extremely reactive under both acidic and neutral conditions. That is, its dimer and trimer usually coexist[11,43] (Figure 2c). Since only the monomer can be easily metabolized by cells for producing pelletierine, direct addition of Δ^1-piperideine into the fermentation medium is presumably cost-ineffective. Apart from this concern, the fate of Δ^1-piperideine after it enters cells is uncertain. To reduce production cost and mitigate uncertainty, we thereby intensified the intracellular biosynthesis of Δ^1-piperideine from L-lysine via three successive reactions: first, L-lysine was decarboxylated by LDC (EC 4.1.1.18, encoded by *LDC*) to form cadaverine;[42,44,45] next, cadaverine was oxidized by CAO (EC 1.4.3.21, encoded by *CAO*) to form 5-aminopentanal; lastly, 5-aminopentanal underwent spontaneous cyclization to form Δ^1-piperideine.[11,15] Considering that LDC and CAO are key enzymes for Δ^1-piperideine biosynthesis, they were overexpressed, and the corresponding recombinant strain *E. coli*(pET-CAO-LDC) was cultivated in M9 medium supplemented with glucose and L-lysine. After 3 h of shake-flask cultivation, 0.5 mM IPTG, 0.05 mM PLP,[34] and 0.05 mM TPQ were added to induce protein expression. Compared with wild-type *E. coli*, this recombinant strain produced more Δ^1-piperideine. Although LC−MS analysis revealed the concurrence of the dimer and trimer of Δ^1-piperideine because of high reactivity even at pH

https://doi.org/10.1021/acssuschemeng.4c05975
ACS Sustainable Chem. Eng. 2025, 13, 778−790

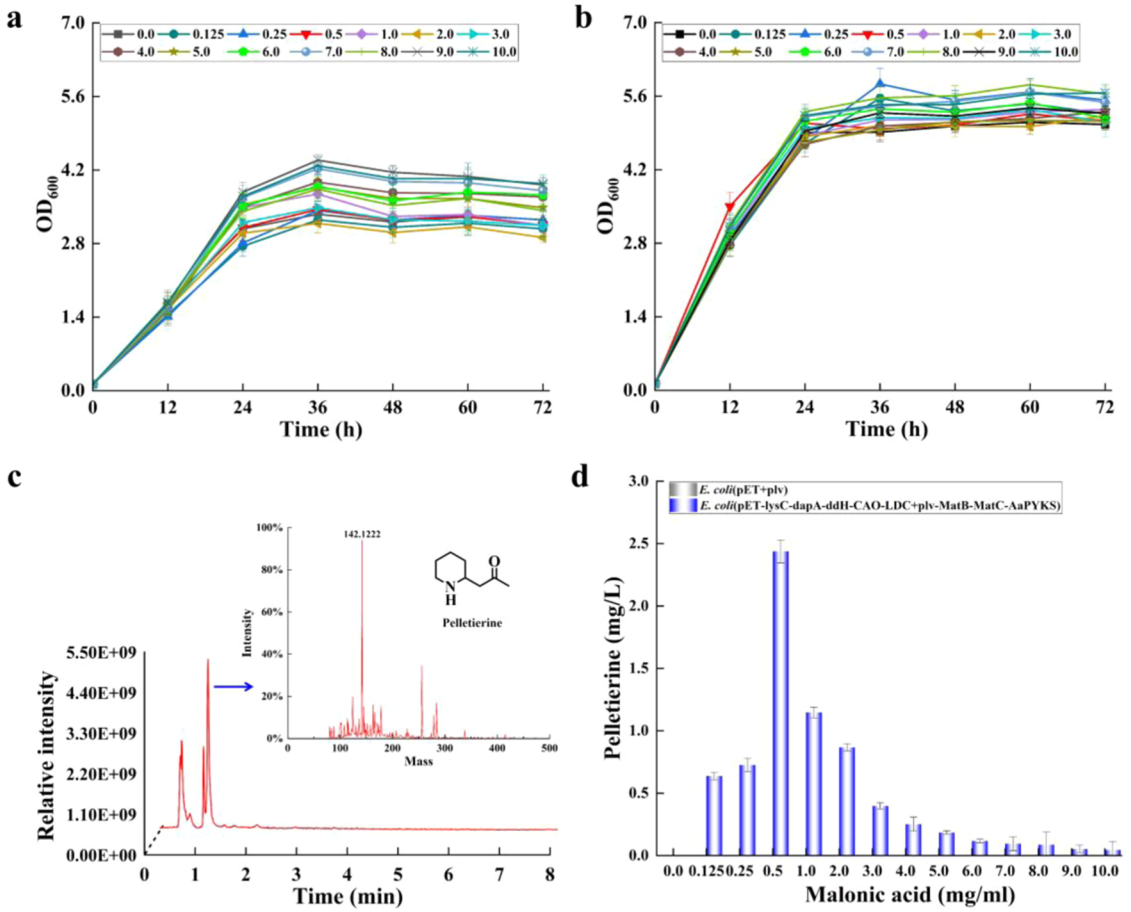

Figure 3. Optimization of the malonic acid concentration for improving pelletierine production in recombinant strains. (a) Growth curve of the control strain *E. coli*(pET+plv) at different concentrations of malonic acid. (b) Growth curve of the recombinant strain *E. coli*(pET-lysC-dapA-ddh-CAO-LDC+plv-matB-matC-AaPYKS) at different concentrations of malonic acid. (c) LC−MS analysis of standard pelletierine. The inset shows the mass spectrometry chromatogram of pelletierine. (d) LC−MS analysis of pelletierine in the 72 h fermentation broth of *E. coli*(pET + plv) and *E. coli*(pET-lysC-dapA-ddh-CAO-LDC + plv-matB-matC-AaPYKS) with different concentrations of malonic acid. *E. coli*(pET + plv), recombinant *E. coli* strain harboring vectors pET and plv. *E. coli*(pET-lysC-dapA-ddh-CAO-LDC + plv-matB-matC-AaPYKS), recombinant *E. coli* strain harboring vectors pET-lysC-dapA-ddh-CAO-LDC and plv-matB-matC-AaPYKS. The results represent the mean ± s.d. of triplicates (n = 3).

7.0[11,43] (Figure 2c,2g), Δ^1-piperideine was still successfully monitored by LC−MS, indicating that the strain *E. coli*(pET-CAO-LDC) was able to synthesize Δ^1-piperideine.

***De Novo* Biosynthesis of Δ^1-Piperideine from Glucose.** Encouraged by the fact that the aforementioned two modules could produce L-lysine and Δ^1-piperideine, respectively, we next combined them for *de novo* biosynthesis of Δ^1-piperideine from glucose. Briefly, we constructed the vector pET-lysC-dapA-ddh-CAO-LDC in which the *LDC* and *CAO* genes for Δ^1-piperideine biosynthesis were coexpressed with the *lysC*, *dapA*, and *ddh* genes for L-lysine biosynthesis. The corresponding recombinant strain *E. coli*(pET-lysC-dapA-ddh-CAO-LDC) was cultivated in a shake-flask with glucose as the carbon source to examine the effect of coexpressing five genes (*lysC*, *dapA*, *ddh*, *LDC*, and *CAO*) on Δ^1-piperideine production. LC−MS analysis showed that both the strain *E. coli*(pET-lysC-dapA-ddh-CAO-LDC) and the strain *E. coli*Δ-*speG*(pET-lysC-dapA-ddh-CAO-LDC) produced much more Δ^1-piperideine compared to the control strain *E. coli*(pET) (Figure 2d−2f), indicating that the two modules can be merged for the *de novo* biosynthesis of Δ^1-piperideine from glucose.

Performance of the 3-Oxoglutaryl Ketide Module. In this module, malonic acid underwent reactions to form malonyl-CoA.[46] Afterward, two molecules of malonyl-CoA were catalyzed into one molecule of 3-oxoglutaryl ketide by polyketide synthase. Since malonyl-CoA is a metabolic hub and rapidly converts into other metabolites,[33] its innate intracellular level is rather low. Presumably, this substrate paucity curtails the catalytic activity of PKS[31,32] and therefore impedes 3-oxoglutaryl ketide biosynthesis. Fortunately, the malonyl-CoA synthetase (MatB, CAE25665.1, encoded by *matB*) from *Arabidopsis thaliana* can efficiently catalyze free malonate and CoA to form malonyl-CoA,[30,47] and a putative malonate carrier protein (MatC, AAC45458.1, encoded by *matC*) from *Rhizobium trifolii* can transfer malonate into *E. coli*.[30] Thus, the *matC* and *matB* genes were coexpressed to elevate the intracellular malonyl-CoA concentration. As anticipated, the corresponding recombinant strain *E. coli*(plv-matB-matC) showed improved production of malonyl-CoA, which was successfully monitored by the malonyl-CoA immunoassay kit. In contrast, the control strain *E. coli*(plv) produced rather less malonyl-CoA, which could not be monitored by this kit (Figure S1).

https://doi.org/10.1021/acssuschemeng.4c05975
ACS Sustainable Chem. Eng. 2025, 13, 778−790

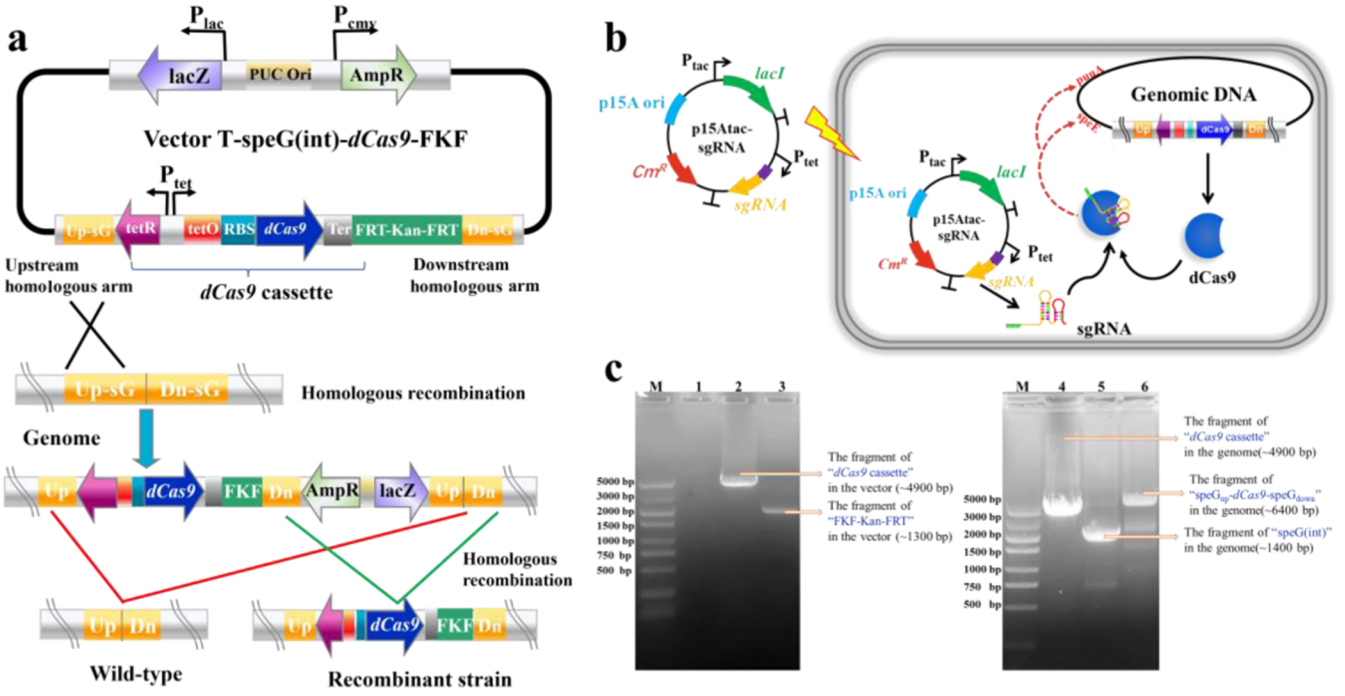

Figure 4. Engineering the CRISPRi system in *E. coli*. (a) Lambda Red homologous recombination-mediated insertion of *the dCas9* cassette into the *speG* gene in the *E. coli* genome. FRT-Kan-FRT (FKF) fragment, *dCas9* cassette, *tet* promoter, *tet* operon. (b) Schematic diagram of engineering the CRISPRi system in *E. coli*. (c) Colony PCR analysis of recombinant *E. coli* strains. M: DNA marker; lanes 1−4: PCR amplification of the *dCas9* expression cassette and FRT-Kan-FRT fragment; lanes 5−6: PCR amplification of the *speG* fragment using primers flanking "speG(int)"; lanes 1 and 5: genomic DNA of wild-type *E. coli*; lanes 2 and 3: DNA fragments of the vector T-speG(int)-*dCas9*-FKF; lanes 4 and 6: genomic DNA of recombinant *E. coli* with the *dCas9* cassette inserted in the genome.

Given that the strain *E. coli*(plv-matB-matC) could biosynthesize malonyl-CoA, we then sought to convert malonyl-CoA into 3-oxoglutaryl ketide. To achieve this, a high activity of PKS is needed. Considering the challenge of expressing plant enzymes in *E. coli*, we examined a total of three pyrrolidine ketide synthases (PYKs), including *Ab*PYKS (encoded by *AbPYKS*, GenBank MH292963),[32] *Ab*PKS2 (encoded by *AbPKS2*, GenBank MN025474),[31] and *Aa*PYKS (encoded by *AaPYKS*, GenBank MN025472)[31] from *Atropa belladonna*, *Aloe barbadensis,* and *Anisodus acutangulus*, respectively. At last, *Aa*PYKS was chosen to catalyze the formation of 3-oxoglutaryl ketide, as it is an unusual plant PKS III catalyzing one round of malonyl CoA condensation. Surprisingly, when *AaPYKS* was coexpressed with the *matC* and *matB* genes for biosynthesis of 3-oxoglutaryl ketide in *E. coli*, 3-oxoglutaryl ketide was not monitored by LC−MS from a shake-flask fermentation broth. This was likely due to its rapid degradation at room temperature and difficulty in ionization. To circumvent this dilemma, we gave up direct detection of 3-oxoglutaryl ketide. Instead, we detected the formation of pelletierine. To this end, we combined the 3-oxoglutaryl ketide module and Δ^1-piperideine module to see if the corresponding recombinant strain could produce pelletierine (Figure 1b). Fortunately, pelletierine was successfully detected by LC−MS from the strain carrying the aforementioned two modules (Figure 3c,3d). In contrast, pelletierine was not monitored by LC−MS from the control strains devoid of *Aa*PYKS, including the strain harboring an empty vector and the strains overexpressing *Ab*PYKS or *Ab*PKS2. These findings suggested that *Aa*PYKS is necessary for the biosynthesis of 3-oxoglutaryl ketide. To exclude the possibility that other metabolites might interact with Δ^1-piperideine to form pelletierine, we added chemically synthesized pure 3-oxoglutaryl ketide (despite rapid degradation) to the fermentation broth of the strain carrying the Δ^1-piperideine module but without the 3-oxoglutaryl ketide module. As anticipated, pelletierine was successfully monitored by LC−MS, indicating that only the 3-oxoglutaryl ketide produced by the corresponding module interacted with Δ^1-piperideine to form pelletierine. The above results suggested that the strain coexpressing *AaPYKS*, *matC*, and *matB* genes was able to synthesize 3-oxoglutaryl ketide, and the *Aa*PYKS functioned properly in this module.

Performance of the Pelletierine Module. Given that both the Δ^1-piperideine module and 3-oxoglutaryl ketide module functioned properly, as mentioned earlier, they were simultaneously introduced into *E. coli* to biosynthesize pelletierine. Malonic acid as a substrate was directly added into shake-flasks. Considering that malonic acid is a crucial substrate of 3-oxoglutaryl ketide, we optimized its concentration. Briefly, the recombinant strain *E. coli*(pET-lysC-dapA-ddh-CAO-LDC + plv-matB-matC-AaPYKS) was grown in shake-flasks, each containing malonic acid at 0.125, 0.25, 0.5, 1.0, 2.0, 3.0, 4.0, 5.0, 6.0, 7.0, 8.0, 9.0, or 10.0 mg/mL, and the strain *E. coli*(pET + plv) was used as the control. Remarkably, at pH 7.0, the strain *E. coli*(pET-lysC-dapA-ddh-CAO-LDC + plv-matB-matC-AaPYKS) showed enhanced growth at various malonic acid concentrations compared to the control strain *E. coli*(pET + plv) (Figure 3a,3b). Additionally, strains *E. coli*(pET + plv) and *E. coli*(pET-lysC-dapA-ddh-CAO-LDC + plv-matB-matC-AaPYKS) grew rapidly at moderate malonic acid concentrations (Figure 3a,b). LC−MS analysis revealed that when malonic acid concentration was 0.5 mg/mL, the strain presented the highest pelletierine production (2.44 mg/L) at 72 h (Figure 3c,3d), indicating that 0.5 mg/mL malonic

https://doi.org/10.1021/acssuschemeng.4c05975
ACS Sustainable Chem. Eng. 2025, 13, 778−790

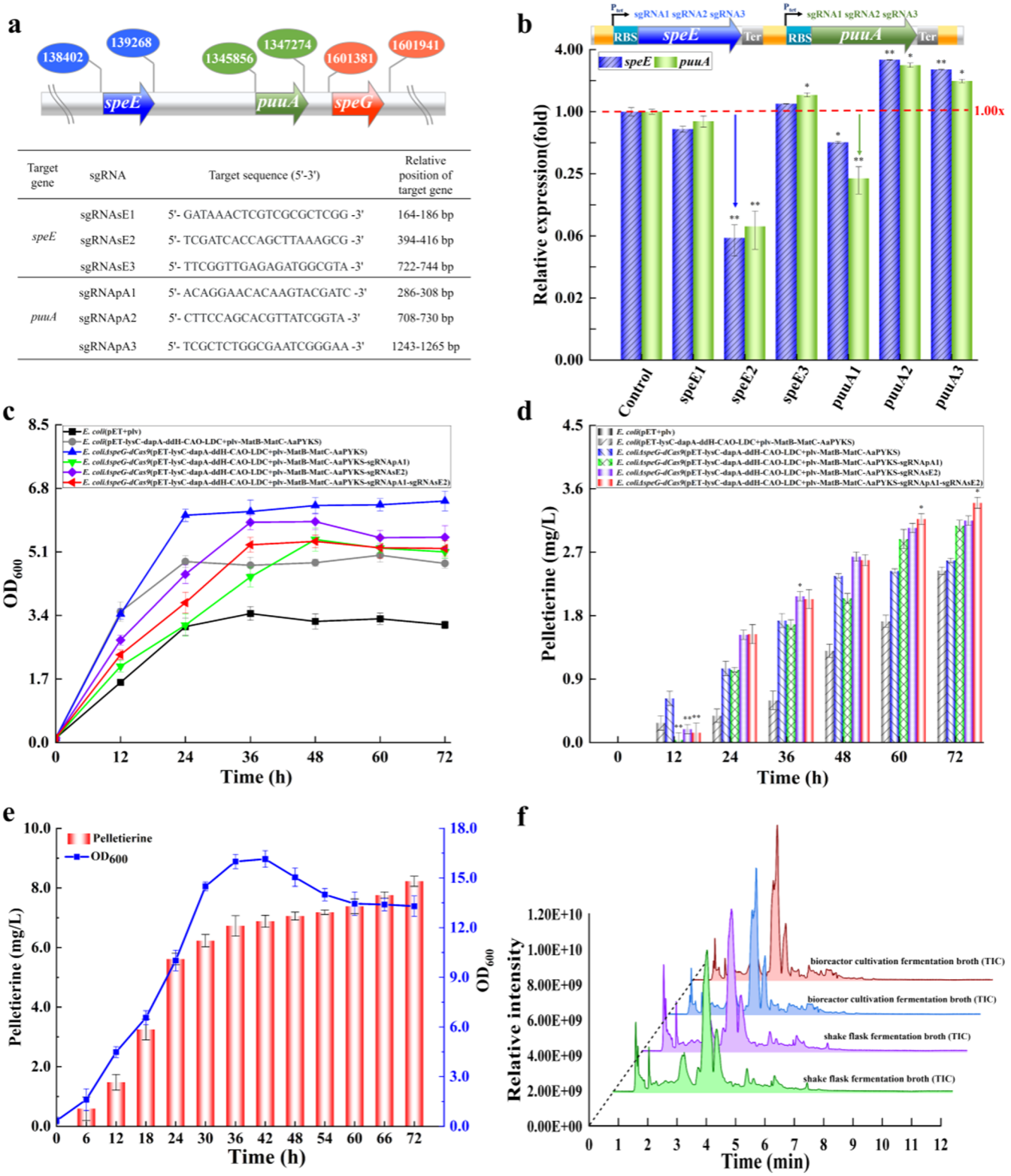

Target gene	sgRNA	Target sequence (5'-3')	Relative position of target gene
speE	sgRNAsE1	5'- GATAAACTCGTCGCGCTCGG -3'	164-186 bp
	sgRNAsE2	5'- TCGATCACCAGCTTAAAGCG -3'	394-416 bp
	sgRNAsE3	5'- TTCGGTTGAGAGATGGCGTA -3'	722-744 bp
puuA	sgRNApA1	5'- ACAGGAACACAAGTACGATC -3'	286-308 bp
	sgRNApA2	5'- CTTCCAGCACGTTATCGGTA -3'	708-730 bp
	sgRNApA3	5'- TCGCTCTGGCGAATCGGGAA -3'	1243-1265 bp

Figure 5. Performance of the CRISPRi system in *E. coli*Δ*speG* strains carrying the pelletierine biosynthesis pathway at 0.5 mg/mL malonic acid concentration. (a) Relative positions of *speE*, *puuA*, and *speG* genes in the *E. coli* genome and the corresponding sgRNA sequences. sgRNAsE1, sgRNAsE2, and sgRNAsE3: three candidate guide RNAs targeting the *speE* gene; sgRNApA1, sgRNApA2, and sgRNApA3: three candidate guide RNAs targeting the *puuA* gene. (b) RT-qPCR analysis of the effects of the CRISPRi system on the expression levels of *speE* and *puuA* genes in the *E. coli*Δ*speG-dCas9* strain. (c), Growth curves of six recombinant strains. (d) LC−MS analysis of pelletierine in recombinant strains after 72 h of shake-flask cultivation. (e) Growth curve and pelletierine production in the recombinant strain *E. coli*Δ*speG-dCas9*(pET-lysC-dapA-ddh-CAO-LDC+plv-matB-matC-AaPYKS-sgRNApA1-sgRNAsE2) after 72 h of fermentation in the 5 L bioreactor. (f) LC−MS (positive ion) total ion chromatograpy (TIC) analysis of fermentation broth of *E. coli*Δ*speG-dCas9*(pET-lysC-dapA-ddh-CAO-LDC + plv-matB-matC-AaPYKS-sgRNApA1-sgRNAsE2) cultivated in the shake-flask and bioreactor. *E. coli*(pET + plv), recombinant *E. coli* strain harboring vectors pET and plv. *E. coli*(pET-lysC-dapA-ddh-CAO-LDC+plv-matB-matC-AaPYKS), recombinant *E. coli* strain harboring vectors pET-lysC-dapA-ddh-CAO-LDC and

https://doi.org/10.1021/acssuschemeng.4c05975
ACS Sustainable Chem. Eng. 2025, 13, 778−790

Figure 5. continued

plv-matB-matC-AaPYKS. *E. coli*Δ*speG-dCas9*, *E. coli* with the mutant *speG* gene and the *dCas9* cassette in the genome; *E. coli*Δ*speG-dCas9*(pET-lysC-dapA-ddh-CAO-LDC + plv-matB-matC-AaPYKS), recombinant *E. coli*Δ*speG-dCas9* strain harboring vectors pET-lysC-dapA-ddh-CAO-LDC and plv-matB-matC-AaPYKS; *E. coli*Δ*speG-dCas9*(pET-lysC-dapA-ddh-CAO-LDC+plv-matB-matC-AaPYKS-sgRNApA1), recombinant *E. coli*Δ*speG-dCas9* strain harboring vectors pET-lysC-dapA-ddh-CAO-LDC and plv-matB-matC-AaPYKS-sgRNApA1; *E. coli*Δ*speG-dCas9*(pET-lysC-dapA-ddh-CAO-LDC+plv-matB-matC-AaPYKS-sgRNAsE2), recombinant *E. coli*Δ*speG-dCas9* strain harboring vectors pET-lysC-dapA-ddh-CAO-LDC and plv-matB-matC-AaPYKS-sgRNAsE2; *E. coli*Δ*speG-dCas9*(pET-lysC-dapA-ddh-CAO-LDC+plv-matB-matC-AaPYKS-sgRNApA1-sgRNAsE2), recombinant *E. coli*Δ*speG-dCas9* strain harboring vectors pET-lysC-dapA-ddh-CAO-LDC and plv-matB-matC-AaPYKS-sgRNApA1-sgRNAsE2. The results represent the mean ± s. d. of triplicates (n = 3). *P < 0.05; **P < 0.01.

acid was appropriate for pelletierine production (Figure 3d). The above results suggest that pelletierine was successfully biosynthesized by the aforementioned four modules in *E. coli*.

Effects of the CRISPRi System on Byproduct Formation in Competing Pathways. In the Δ^1-piperideine module for pelletierine production, although the overexpression of CAO converted most cadaverine to 5-aminopentanal, partial cadaverine was still converted to glutamyl cadaverine, aminopropyl cadaverine, and *N*-acetyl-cadaverine, which are three byproducts whose formation are catalyzed by enzymes PuuA (EC 6.3.1.11, encoded by *puuA*), SpeE (EC 2.5.1.16, encoded by *speE*), and SpeG (EC 2.3.1.57, encoded by *speG*), respectively. To diminish the three byproducts, we engineered a CRISPRi system with expectation that the *speG* gene was disrupted by insertion of the *dCas9* expression cassette, and the *puuA* and *speE* genes were inhibited by the sgRNA−dCas9 complex (Figures 1b, 4, and 5). To do so, the *dCas9* expression cassette was inserted into the *speG* gene in the *E. coli* genome via Red homologous recombination (Figure 4a,4b). PCR amplification using primers flanking the *speG* gene and subsequent DNA sequencing revealed 100% identity of the cloned *dCas9* fragment to the reported sequence in GenBank (Figure 4c, lanes 5 and 6). In contrast, no fragments were cloned from the wild-type *E. coli* genome (Figure 4c, lane 1). These results suggested that the *dCas9* cassette was inserted into the *speG* gene in the *E. coli* genome. Subsequently, we investigated the effects of *speG* gene disruption on the biosynthesis of Δ^1-piperideine and pelletierine. Since Δ^1-piperideine is extremely reactive, it coexists with its dimer and trimer. Hence, it is challenging to accurately determine their proportions. However, considering the control strain and the two recombinant strains *E. coli*(pET-lysC-dapA-ddh-CAO-LDC) and *E. coli*Δ*speG*(pET-lysC-dapA-ddh-CAO-LDC) were derived from the same host and the only difference between the two recombinant strains is deletion of the *speG* gene or not, the data points of the LC−MS chromatogram and the relative intensity can thus reflect the proportion of Δ^1-piperideine in the mixture (Figures S4−S7). Interestingly, LC−MS analysis of fermentation broth showed that the strain *E. coli*Δ*speG*(-pET-lysC-dapA-ddh-CAO-LDC) with the disrupted *speG* gene produced more Δ^1-piperideine and its dimer compared to the strain *E. coli*(pET-lysC-dapA-ddh-CAO-LDC) with intact *speG* gene (Figure 2e,2f). In addition, after 72 h of shake-flask cultivation, the strain *E. coli*Δ*speG*(pET-lysC-dapA-ddh-CAO-LDC+plv-matB-matC-AaPYKS) with the disrupted *speG* gene produced 2.58 mg/L pelletierine, which was a 5.74% enhancement compared to 2.44 mg/L produced by *E. coli*(pET-lysC-dapA-ddh-CAO-LDC+plv-matB-matC-AaPYKS) with intact *speG* gene (Figure 5d). These results suggest that the disruption of the *speG* gene benefited the biosynthesis of Δ^1-piperideine and pelletierine.

Given that the *dCas9* expression cassette could knock out the *speG* gene in one competing pathway, we next constructed an sgRNA expression cassette to knock down the *puuA* and *speE* genes in two other competing pathways. Considering that the position of the protospacer adjacent motif (PAM) and the binding of sgRNA to the genome largely affect the CRISPRi efficiency, we designed a total of six candidate sgRNAs (three for targeting *puuA* and other three for targeting *speE*) and examined their inhibition efficiency (Figure 5a,b). The CRISPRi vectors targeting *speE* and *puuA* genes were constructed and transformed into the strain *E. coli-dCas9* (Figure 4b). RT-qPCR analysis showed strong inhibition of the CRISPRi system on *speE* and *puuA* compared to the control. As shown in Figure 5b, the CRISPRi system carrying sgRNAsE2 and sgRNApA1 led to 94 and 77% transcription inhibition, respectively.

Effects of the CRISPRi System on Pelletierine Production by *E. coli* in Shake-Flasks. Given that the engineered CRISPRi system was able to effectively repress *speE* and *puuA* genes (Figure 5b), we then investigated its effect on pelletierine production. In the logarithmic phase of shake-flask fermentation, the *speE* and *puuA* genes were suppressed after ATC was added into the medium to trigger the expression of the *tet* promoter-driven *dCas9* cassette, sgRNAsE2 cassette, sgRNApA1 cassette, and duo of sgRNAsE2 and sgRNApA1. The results showed that the *speE* and *puuA* genes in *E. coli*Δ*speG-dCas9* were downregulated (Figure 5b). Subsequently, shake-flask cultivation was performed to evaluate the synergistic effects of *speG* disruption and CRISPRi downregulation by the sgRNAsE2 cassette, the sgRNApA1 cassette, or the duo of sgRNAsE2 and sgRNApA1 cassettes on pelletierine production. As shown in Figure 5c, the control strain *E. coli*(pET + plv) grew slowly, and its biomass was comparable to wild-type *E. coli*. In contrast, the recombinant strain *E. coli*(pET-lysC-dapA-ddh-CAO-LDC + plv-matB-matC-AaPYKS) following a pelletierine biosynthesis pathway displayed enhanced growth but did not reach an optimal level, suggesting that the engineered pelletierine biosynthesis pathway benefits cell growth, albeit unknown biological limiting factors. Strikingly, the strain *E. coli*Δ*speG*(pET-lysC-dapA-ddh-CAO-LDC + plv-matB-matC-AaPYKS) showed the fastest growth. This was presumably ascribed to the disruption of the *speG* gene and metabolic flux reallocation. Interestingly, the three CRISPRi strains showed similar levels of OD_{600} but lower OD_{600} compared to the strain devoid of the sgRNA expression cassette. This finding indicated that the sgRNA expression cassette exerted a stress on cell growth. Despite this pitfall, after 60 h of cultivation, the three strains carrying both the CRISPRi system and pelletierine biosynthesis pathway produced more pelletierine than the strain only carrying pelletierine biosynthesis pathway. As shown in Figure 5d, the five recombinant strains *E. coli*(pET-lysC-dapA-ddh-CAO-

https://doi.org/10.1021/acssuschemeng.4c05975
ACS Sustainable Chem. Eng. 2025, 13, 778−790

LDC + plv-matB-matC-AaPYKS), *E. coli*Δ*speG*(pET-lysC-dapA-ddh-CAO-LDC + plv-matB-matC-AaPYKS), *E. coli*Δ*speG-dCas9*(pET-lysC-dapA-ddh-CAO-LDC + plv-matB-matC-AaPYKS-sgRNApA1), *E. coli*Δ*speG-dCas9*(pET-lysC-dapA-ddh-CAO-LDC + plv-matB-matC-AaPYKS-sgRNAsE2), and *E. coli*Δ*speG-dCas9*(pET-lysC-dapA-ddh-CAO-LDC + plv-matB-matC-AaPYKS-sgRNApA1-sgRNAsE2) produced 2.44, 2.58, 3.07, 3.15, and 3.40 mg/L pelletierine following 72 h of cultivation, respectively. Clearly, the disruption of the *speG* gene and the sgRNA expression cassette benefited pelletierine production, and the sgRNAsE2 cassette outperformed the sgRNApA1 cassette in this regard. Compared to the strain only carrying the sgRNAsE2 or sgRNApA1 cassette, the strain carrying both sgRNAsE2 and sgRNApA1 cassettes produced more pelletierine (Figure 5d). The above results indicated that disrupting the *speG* gene in alliance with inhibiting *puuA* and *speE* genes by the CRISPRi system was more effective in improving pelletierine production (3.40 mg/L) compared to scenarios with the intact *speG* gene (2.44 mg/L) and disrupted *speG* gene (2.58 mg/L) (Figure 5d).

Bioreactor Cultivation. Given the noticeable ability of *E. coli*Δ*speG-dCas9*(pET-lysC-dapA-ddh-CAO-LDC + plv-matB-matC-AaPYKS-sgRNApA1-sgRNAsE2) to produce pelletierine in a shake-flask, we next investigated its performance in a 5 L bioreactor. Based on pre-experiments, inducers (IPTG and ATC) and cofactors (PLP and TPQ) were added during the late stage of logarithmic phase. To alleviate metabolic stress and boost pelletierine production, glucose and malonic acid were replenished. We found that pelletierine was rapidly produced in the following 18 h, presumably due to available Δ^1-piperideine and 3-oxoglutaryl ketide. As shown in Figure 5e and Table S4, this recombinant *E. coli* strain produced 8.23 mg/L pelletierine with 1.77 mg/g yield and 0.11 mg/(L h) productivity at 72 h. That is, this recombinant strain showed 142 and 120% enhancement in titer and productivity, respectively, as compared to 3.40 and 0.05 mg/L/h in shake-flask fermentation. However, during the late stage of fermentation, although the pelletierine level was stable, cell growth was halted. This might be attributed to the formation of byproducts. Nevertheless, the replenishment of glucose and malonic acid improved the cell growth and accordingly boosted pelletierine production. To further improve pelletierine production, limiting factors need to be discovered. To this end, shake-flask and bioreactor fermentation broth were analyzed using the total ion chromatogram (TIC). Unfortunately, no significant difference was observed (Figure 5f).

DISCUSSION

In this study, glucose-based biosynthesis of pelletierine was realized by engineering four modules in *E. coli* (Figure 1b), including an L-lysine module for converting glucose to L-lysine, a Δ^1-piperideine module for converting L-lysine to Δ^1-piperideine, a 3-oxoglutaryl ketide module for converting malonic acid to 3-oxoglutaryl ketide, and a pelletierine module for converting 4-(2-piperidyl)-acetoacetic acid to pelletierine. To boost pelletierine production, the genes *lysC*, *dapA*, *ddh*, *CAO*, and *LDC* were overexpressed, and the genes *speG*, *speE*, and *puuA* in competing pathways were knocked out or knocked down by the engineered CRISPRi system (Figure 4). The *dCas9* expression cassette was integrated into the *E. coli* genome to not only disrupt the *speG* gene in one competing pathway but also mitigate vector burden (Figure 4b,c). To elevate the intracellular 3-oxoglutaryl ketide level, the transporter MatC, malonyl-CoA synthetase MatB, and high-activity *Aa*PYKS were overexpressed. Relying on aforementioned manipulations, the resulting strain *E. coli*Δ*speG-dCas9*(pET-lysC-dapA-ddh-CAO-LDC+plv-matB-matC-AaPYKS-sgRNA-pA1-sgRNAsE2) harboring two distinct vectors produced 3.40 mg/L (Figure 5d) and 8.23 mg/L (Figure 5e) pelletierine in the shake-flask and 5 L bioreactor, respectively. To our knowledge, this is the first report of the microbial production of pelletierine.

In the recombinant *E. coli* strain harboring two vectors, the production of pelletierine was jointly accomplished by 3 plant genes (*AbPYKS*, *AbPKS2*, and *AaPYKS* from *A. belladonna*, *A. barbadensis*, and *A. acutangulus*, respectively), 7 key genes native to *E. coli*, and 3 genes from other bacteria (*ddh*, *matB*, and *matC* genes from *C. glutamicum*, *Rhodopseudomonas palustris*, and *Klebsiella pneumoniae*, respectively) (Figure 1b). Presumably, high-level production of pelletierine was hindered by at least five obstacles. First, heterologous expression of these genes exerts a heavy metabolic burden on the host *E. coli*.[48] This burden could be mitigated by multicopy integration of these genes into the genome. Second, inadequate or excessive expression of key genes (e.g., *lysC*, *dapA*, and *ddh*) may curb pelletierine biosynthesis. This could be tackled by promoter substitution or enzyme modification. Third, heterologous expression of plant-derived enzymes in *E. coli* generally encounters codon mismatch, which hampers gene expression and pelletierine formation. This obstacle could be overcome by codon optimization and modification of th ePKS gene cluster,[49,50] as the two strategies influence post-translation modification and subcellular localization.[48,51] Fourth, promiscuous reactions may occur in the L-lysine module, Δ^1-piperideine module, and 3-oxoglutaryl ketide module, which not only bring about protein aggregation but also impede the intrinsic pathways in *E. coli*. For instance, the malonyl-CoA in 3-oxoglutaryl ketide module is a branch node relating to not only 3-oxoglutaryl ketide biosynthesis but also the metabolisms of cholesterol and fatty acids.[52,53] Clearly, the versatility of malonyl-CoA attenuates 3-oxoglutaryl ketide biosynthesis. To abate unwanted reactions, the engineered modules could be tinkered by CRISPR tools, base editing, or prime editing. Fifth, the biosynthesis of pelletierine from glucose and L-aspartate involves approximately 21 and 11 reactions, respectively. Due to the participation of multiple enzymes, a powerful driving force is of paramount importance for the high-level production of pelletierine. In this regard, beyond conventional strategies such as inducible expression and timely attenuation of feedback inhibition, pelletierine could also be overproduced through coupling its biosynthetic pathway with cell growth pathways (e.g., TCA cycle) by sharing promoters or recycling cofactors for each other, given that cell growth is the fundamental driving force of biosynthesis. This viewpoint was actually supported by this present study. As shown in Figure 2b, the overexpression of the *ddh* gene in the L-lysine module improved not only *E. coli* growth but also pelletierine production. Presumably, pelletierine production was to some extent coupled with *E. coli* growth. To better understand this coupling, pelletierine could be extracted from fermentation broth by an efficient hybrid-integrated membrane separation,[54] and this separation system comprises microfiltration (removal of cells), ultrafiltration (removal of proteins), and reverse osmosis (recovery, preconcentration, and prepurification of pelletierine). We anticipate that timely removal of pelletierine can attenuate its stress on cell growth, which, in turn, benefits

https://doi.org/10.1021/acssuschemeng.4c05975
ACS Sustainable Chem. Eng. 2025, 13, 778−790

pelletierine production. Namely, except for the coupling, there exists a competition between pelletierine production and cell growth for cellular resources. Apart from aforementioned five obstacles, biosynthesis of pelletierine involves both amino acid and polyketide metabolisms.[10,11] Hence, fine regulation is required to reallocate metabolic fluxes, and this mission could be accomplished using an arsenal of tools such as CRISPRi, base editing, and epigenome editing.

So far, the enzymes participating in HupA biosynthesis have not been completely identified. For instance, how pelletierine and 4PAA act together to form the carbon scaffold of HupA remains poorly understood.[11] While isotope tracing is a conventional approach to decipher biosynthesis pathways, RNA sequencing of HupA-producing *Hydrangea serrata* along with bioinformatics analysis may shed light on this "black box".[8,11] To date, the reported key enzymes for complete biosynthesis of HupA include short-chain dehydrogenase/reductase (SDR), BAHD acyl transferase (ACT), cytochrome P450 (CYP782C1), α carbonic anhydrase (CAL), Fe(II)/2-OG-dependent dioxygenases (2OGDs), and α/β hydrolase (ABH)[8] (Figure S2). Although most of them have been experimentally validated by transient expression in *Nicotiana benthamiana*, the enzyme catalyzing the formation of flabellidine, a precursor of HupA, remains enigmatic. It has been reported that 7-methyl-5-(((*S*)-piperidin-2-yl)methyl)-2,3,4,6,7,8-hexahydroquinoline (7M5PHQ) and flabellidine are two metabolites connecting pelletierine to HupA (Figure S2), and flabellidine is likely derived from 7M5PHQ (Figure S3). However, 7M5PHQ is highly reactive and thereby cannot be catalyzed into flabellidine by extant enzymes unless there is extensive optimization of experimental conditions. One exhilarating prediction is that acetyltransferases can catalyze the final step of flabellidine formation.[8] Although in-depth studies are needed to validate this prediction, the gap between 7M5PHQ and flabellidine could be bridged soon by means of transcriptome analysis, machine learning-based prediction, as well as function validation. Overall, this study contributed to future complete biosynthesis of HupA. More broadly, this study has provided a basis for sustainable production of other derivatives of pelletierine.

■ ASSOCIATED CONTENT

Supporting Information

The Supporting Information is available free of charge at https://pubs.acs.org/doi/10.1021/acssuschemeng.4c05975.

Cell growth and malonyl-CoA production of strains *E. coli* (plv) and *E. coli* (plv-matB-matC); huperzine A biosynthetic pathway from pelletierine; putative biosynthesis of flabellidine from 7-(methyl-5-((*S*)-piperidin-2-yl)methyl)-2,3,4,6,7,8-hexahydroquinoline; LC−MS analysis of Δ^1-piperideine from the fermentation broth of strain *E. coli*(pET), *E. coli*(pET-lysC-dapA-ddh-CAO-LDC), *E. coli*ΔspeG(pET-lysC-dapA-ddh-CAO-LDC), and standard Δ^1-piperideine; details of plasmids and strains; primers used in this study; pathway genes and the corresponding GenBank accession numbers; and titer, yield, and productivity of pelletierine produced by the strain *E. coli*ΔspeG-dCas9(pET-lysC-dapA-ddh-CAO-LDC+plv-matB-matC-AaPYKS-sgRNAPA1-sgRNAsE2) in the shake-flask and bioreactor (PDF)

■ AUTHOR INFORMATION

Corresponding Author

Pingfang Tian − *Beijing Key Laboratory of Bioprocess, College of Life Science and Technology, Beijing University of Chemical Technology, Beijing 100029, P. R. China;* orcid.org/0000-0001-5261-9516; Email: tianpf@mail.buct.edu.cn

Authors

Wei Li − *Beijing Key Laboratory of Bioprocess, College of Life Science and Technology, Beijing University of Chemical Technology, Beijing 100029, P. R. China*

Peng Zhao − *College of Bioscience and Resources Environment, Beijing University of Agriculture, Beijing 102206, P. R. China*

Ying Li − *College of Biochemical Engineering, Beijing Union University, Beijing 100023, P. R. China;* orcid.org/0000-0001-8321-022X

Shimin Wu − *Beijing Key Laboratory of Bioprocess, College of Life Science and Technology, Beijing University of Chemical Technology, Beijing 100029, P. R. China*

Complete contact information is available at: https://pubs.acs.org/10.1021/acssuschemeng.4c05975

Author Contributions

P.T. and W.L. conceived and designed the experiments. W.L. performed the experiment. P.Z., Y.L., and S.W. analyzed the data. P.T. supervised the study and wrote the manuscript. All authors have read and approved the final manuscript.

Notes

The authors declare no competing financial interest.

■ ACKNOWLEDGMENTS

This study was funded by grants from the National Key Research and Development Program of China (2018YFA0901800 and 2023YFA0914700) and National Natural Science Foundation of China (22278022).

■ REFERENCES

(1) Johnson, E. C. B.; Bian, S.; Haque, R. U.; Carter, E. K.; Watson, C. M.; Gordon, B. A.; Ping, L.; Duong, D. M.; Epstein, M. P.; McDade, E.; Barthélemy, N. R.; Karch, C. M.; Xiong, C.; Cruchaga, C.; Perrin, R. J.; Wingo, A. P.; Wingo, T. S.; Chhatwal, J. P.; Day, G. S.; Noble, J. M.; Berman, S. B.; Martins, R.; Radford, N. R. G.; Schofield, P. R.; Ikeuchi, T.; Mori, H.; Levin, J.; Farlow, M.; Lah, J. J.; Haass, C.; Jucker, M.; Morris, J. C.; Benzinger, T. L. S.; Roberts, B. R.; Bateman, R. J.; Fagan, A. M.; Seyfried, N. T.; Levey, A. I. Cerebrospinal fluid proteomics define the natural history of autosomal dominant Alzheimer's disease. *Nat. Med.* **2023**, *29* (8), 1979−1988.

(2) Gauthier, S.; Webster, C.; Servaes, S.; Morais, J. A.; Neto, P. R. *World Alzheimer Report: Life after Diagnosis: Navigating Treatment, Care and Support*; Alzheimer's Disease International: London, England, 2022.

(3) Ferrari, C.; Sorbi, S. The complexity of Alzheimer's disease: An evolving puzzle. *Physiol. Rev.* **2021**, *101* (3), 1047−1081.

(4) Ossenkoppele, R.; Kant, R. V. D.; Hansson, O. Tau biomarkers in Alzheimer's disease: Towards implementation in clinical practice and trials. *Lancet Neurol.* **2022**, *21* (8), 726−734.

(5) Warfield, A. E.; Gupta, P.; Ruhmann, M. M.; Jeffs, Q. L.; Guidone, G. C.; Rhymes, H. W.; Thompson, M. I.; Todd, W. D. A brainstem to circadian system circuit links Tau pathology to sundowning-related disturbances in an Alzheimer's disease mouse model. *Nat. Commun.* **2023**, *14* (1), No. 5027.

(6) Xiang, J.; Tao, Y.; Xia, Y.; Luo, S.; Zhao, Q.; Li, B.; Zhang, X.; Sun, Y.; Xia, W.; Zhang, M.; Kang, S. S.; Ahn, E. H.; Liu, X.; Xie, F.; Guan, Y.; Yang, J. J.; Bu, L.; Wu, S.; Wang, X.; Cao, X.; Liu, C.;

Zhang, Z.; Li, D.; Ye, K. Development of an α-synuclein positron emission tomography tracer for imaging synucleinopathies. *Cell* **2023**, *186* (16), 3350−3367.e19.
(7) Ma, X.; Gang, D. R. The Lycopodium alkaloids. *Nat. Prod. Rep.* **2004**, *21* (6), 752−772.
(8) Nett, R. S.; Dho, Y.; Tsai, C.; Passow, D.; Grundman, J. M.; Low, Y. Y.; Sattely, E. S. Plant carbonic anhydrase-like enzymes in neuroactive alkaloid biosynthesis. *Nature* **2023**, *624* (7990), 182−191.
(9) Cheng, B.; Song, L.; Chen, F. Huperzine alkaloids: Forty years of total syntheses. *Nat. Prod. Rep.* **2024**, *41* (1), 59−84.
(10) Li, X.; Li, W.; Tian, P.; Tan, T. Delineating biosynthesis of huperzine A, A plant-derived medicine for the treatment of Alzheimer's disease. *Biotechnol. Adv.* **2022**, *60*, No. 108026.
(11) Nett, R. S.; Dho, Y.; Low, Y. Y.; Sattely, E. S. A metabolic regulon reveals early and late acting enzymes in neuroactive Lycopodium alkaloid biosynthesis. *Proc. Natl. Acad. Sci. U.S.A.* **2021**, *118* (24), No. e2102949118.
(12) Zaidan, R. K.; Evans, P. Strategies for the asymmetric construction of pelletierine and its use in the synthesis of sedridine, myrtine, and lasubine. *Eur. J. Org. Chem.* **2019**, *2019* (32), 5354−5367.
(13) Carlson, E. C.; Rathbone, L. K.; Yang, H.; Collett, N. D.; Carter, R. G. Improved protocol for asymmetric, intramolecular heteroatom michael addition using organocatalysis: Enantioselective syntheses of homoproline, pelletierine, and homopipecolic acid. *J. Org. Chem.* **2008**, *73* (13), 5155−5158.
(14) Yan, L. H.; Dagorn, F.; Gravel, E.; Méniel, B. S.; Poupon, E. Synthesis and reactivity of pelletierine-derived building blocks and pelletierine analogs. *Tetrahedron* **2012**, *68* (31), 6276−6283.
(15) Wang, J.; Zhang, Z. K.; Jiang, F. F.; Qi, B. W.; Ding, N.; Hnin, S. Y. Y.; Liu, X.; Li, J.; Wang, X.; Tu, P. F.; Abe, I.; Morita, H.; Shi, S. P. Deciphering the biosynthetic mechanism of pelletierine in Lycopodium alkaloid biosynthesis. *Org. Lett.* **2020**, *22* (21), 8725−8729.
(16) Braekman, J. C.; Gupta, R. N.; Maclean, D. B.; Spenser, I. D. Biosynthesis of Lycopodine. Pelletierine as an obligatory intermediate. *Can. J. Chem.* **1972**, *50* (16), 2591−2602.
(17) Cope, A. C.; Overberger, C. G. The synthesis of cyclo-öctatetraene from pseudopelletierine. *J. Am. Chem. Soc.* **1947**, *69* (4), No. 976.
(18) Cope, A. C.; Overberger, C. G. Cyclic polyolefins; synthesis of cyclooctatetraene from pseudopelletierine. *J. Am. Chem. Soc.* **1948**, *70* (4), 1433−1437.
(19) Eric Gershwin, M.; Terr, A. Alternative and complementary therapy for asthma. *Clin. Rev. Allergy Immunol.* **1996**, *14* (3), 241−245.
(20) Nuguri, S.; Eppakayala, L.; Vuppula, N. K.; Rajasekhara, P. K. A simple and efficient stereoselective total synthesis of (L)-sedridine. *Int. J. Chem. Anal. Sci.* **2013**, *4* (2), 131−135.
(21) Torres, J.; Escolano, M.; Alcañiz, F. R.; Vidal, A. S.; Roselló, M. S.; Pozo, Cd. Highly convergent total synthesis of (+)-anaferine and (−)-dihydrocuscohygrine. *Org. Chem. Front.* **2019**, *6* (18), 3210−3214.
(22) Beng, T. K.; Gawley, R. E. Highly enantioselective catalytic dynamic resolution of N-Boc-2-lithiopiperidine: Synthesis of (R)-(+)-N-Boc-pipecolic acid, (S)-(−)-coniine, (S)-(+)-pelletierine, (+)-beta-conhydrine, and (S)-(−)-ropivacaine and formal synthesis of (−)-lasubine II and (+)-cermizine C. *J. Am. Chem. Soc.* **2010**, *132* (35), 12216−12217.
(23) Xu, X.; Liu, Y.; Du, G.; Amaro, R. L.; Liu, L. Microbial chassis development for natural product biosynthesis. *Trends Biotechnol.* **2020**, *38* (7), 779−796.
(24) Zhao, C.; Zheng, T.; Feng, Y.; Wang, X.; Zhang, L.; Hu, Q.; Chen, J.; Wu, F.; Chen, G. Q. Engineered *Halomonas* spp. for production of L-lysine and cadaverine. *Bioresour. Technol.* **2022**, *349*, No. 126865.
(25) Li, L.; Li, N.; Wang, X.; Gao, S.; Zhang, J.; Zhou, J.; Wu, Z.; Zeng, W. Metabolic engineering combined with enzyme engineering for overproduction of ectoine in *Escherichia coli*. *Bioresour. Technol.* **2023**, *390*, No. 129862.
(26) Weinstock, M. T.; Jacobsen, M. T.; Kay, M. S. Synthesis and folding of a mirror-image enzyme reveals ambidextrous chaperone activity. *Proc. Natl. Acad. Sci. U.S.A.* **2014**, *111* (32), 11679−11684.
(27) Liu, N.; Zhang, T. T.; Rao, Z. M.; Zhang, W. G.; Xu, J. Z. Reconstruction of the diaminopimelic acid pathway to promote L-lysine production in *Corynebacterium glutamicum*. *Int. J. Mol. Sci.* **2021**, *22* (16), No. 9065.
(28) Gao, X.; Ma, Q.; Chen, M.; Dong, M.; Pu, Z.; Zhang, X.; Song, Y. Insight into the highly conserved and differentiated cofactor-binding sites of *meso*-diaminopimelate dehydrogenase stdapdh. *J. Chem. Inf. Model.* **2019**, *59* (5), 2331−2338.
(29) Sirirungruang, S.; Ad, O.; Privalsky, T. M.; Ramesh, S.; Sax, J. L.; Dong, H.; Baidoo, E. E. K.; Amer, B.; Khosla, C.; Chang, M. C. Y. Engineering site-selective incorporation of fluorine into polyketides. *Nat. Chem. Biol.* **2022**, *18* (8), 886−893.
(30) Liang, B.; Sun, G.; Wang, Z.; Xiao, J.; Yang, J. Production of 3-hydroxypropionate using a novel malonyl-CoA-mediated biosynthetic pathway in genetically engineered *E. coli* strain. *Green Chem.* **2019**, *21* (22), 6103−6115.
(31) Huang, J. P.; Fang, C.; Ma, X.; Wang, L.; Yang, J.; Luo, J.; Yan, Y.; Zhang, Y.; Huang, S. X. Tropane alkaloids biosynthesis involves an unusual type III polyketide synthase and non-enzymatic condensation. *Nat. Commun.* **2019**, *10* (1), No. 4036.
(32) Bedewitz, M. A.; Jones, A. D.; D'Auria, J. C.; Barry, C. S. Tropinone synthesis via an atypical polyketide synthase and P450-mediated cyclization. *Nat. Commun.* **2018**, *9* (1), No. 5281.
(33) Yang, D.; Kim, W. J.; Yoo, S. M.; Choi, J. H.; Ha, S. H.; Lee, M. H.; Lee, S. Y. Repurposing type III polyketide synthase as a malonyl-CoA biosensor for metabolic engineering in bacteria. *Proc. Natl. Acad. Sci. U.S.A.* **2018**, *115* (40), 9835−9844.
(34) Gao, J.; Liu, S.; Zhou, C.; Lara, D.; Zou, Y.; Hai, Y. A pyridoxal 5′-phosphate-dependent Mannich cyclase. *Nat. Catal.* **2023**, *6* (6), 476−486.
(35) Zhang, X.; Wang, Q.; Wu, J.; Wang, J.; Shi, Y.; Liu, M. Crystal structure of human lysyl oxidase-like 2 ($hLOXL_2$) in a precursor state. *Proc. Natl. Acad. Sci. U.S.A.* **2018**, *115* (15), 3828−3833.
(36) Lv, L.; Ren, Y. L.; Chen, J. C.; Wu, Q.; Chen, G. Q. Application of CRISPRi for prokaryotic metabolic engineering involving multiple genes, a case study: Controllable P(3HB-co-4HB) biosynthesis. *Metab. Eng.* **2015**, *29*, 160−168.
(37) Wu, J.; Cheng, Z. H.; Min, D.; Cheng, L.; He, R. L.; Liu, D. F.; Li, W. W. CRISPRi system as an efficient, simple platform for rapid identification of genes involved in pollutant transformation by *Aeromonas hydrophila*. *Environ. Sci. Technol.* **2020**, *54* (6), 3306−3315.
(38) Larson, M. H.; Gilbert, L. A.; Wang, X.; Lim, W. A.; Weissman, J. S.; Qi, L. S. CRISPR interference (CRISPRi) for sequence-specific control of gene expression. *Nat. Protoc.* **2013**, *8* (11), 2180−2196.
(39) Shimizu, Y.; Rai, A.; Okawa, Y.; Tomatsu, H.; Sato, M.; Kera, K.; Suzuki, H.; Saito, K.; Yamazaki, M. Metabolic diversification of nitrogen-containing metabolites by the expression of a heterologous lysine decarboxylase gene in *Arabidopsis*. *Plant J.* **2019**, *100* (3), 505−521.
(40) Sharan, S. K.; Thomason, L. C.; Kuznetsov, S. G.; Court, D. L. Recombineering: A homologous recombination-based method of genetic engineering. *Nat. Protoc.* **2009**, *4* (2), 206−223.
(41) Zhao, P.; Li, Q.; Tian, P.; Tan, T. Switching metabolic flux by engineering tryptophan operon-assisted CRISPR interference system in *Klebsiella pneumoniae*. *Metab. Eng.* **2021**, *65*, 30−41.
(42) Zhou, N.; Wei, G.; Chen, X.; Wu, B.; Li, H.; Lu, Q.; Cao, X.; Zhang, A.; Chen, K.; Ouyang, P. Self-sufficient biocatalysts constructed using chitin-based microspheres. *Chem. Eng. J.* **2023**, *459*, No. 141660.
(43) Mancinotti, D.; Frick, K. M.; Flores, F. G. Biosynthesis of quinolizidine alkaloids in lupins: Mechanistic considerations and prospects for pathway elucidation. *Nat. Prod. Rep.* **2022**, *39* (7), 1423−1437.

https://doi.org/10.1021/acssuschemeng.4c05975
ACS Sustainable Chem. Eng. 2025, 13, 778−790

(44) Xue, Y.; Zhao, Y.; Ji, X.; Yao, J.; Busk, P. K.; Lange, L.; Huang, Y.; Zhang, S. Advances in bio-nylon 5X: Discovery of new lysine decarboxylases for the high-level production of cadaverine. *Green Chem.* **2020**, *22* (24), 8656−8668.
(45) Rui, J.; You, S.; Zheng, Y.; Wang, C.; Gao, Y.; Zhang, W.; Qi, W.; Su, R.; He, Z. High-efficiency and low-cost production of cadaverine from a permeabilized-cell bioconversion by a lysine-induced engineered *Escherichia coli*. *Bioresour. Technol.* **2020**, *302* (9), No. 122844.
(46) Fadó, R.; Rodríguez, R. R.; Casals, N. The return of malonyl-CoA to the brain: Cognition and other stories. *Prog. Lipid Res.* **2021**, *81*, No. 101071.
(47) Krishnan, B. P.; López, L. O. P.; Hoefgen, S.; Xue, L.; Wang, S.; Valiante, V.; Cui, J. Thermomagneto-responsive smart biocatalysts for malonyl-coenzyme A synthesis. *ACS Appl. Mater. Interfaces* **2020**, *12* (18), 20982−20990.
(48) Gao, J.; Zuo, Y.; Xiao, F.; Wang, Y.; Li, D.; Xu, J.; Ye, C.; Feng, L.; Jiang, L.; Liu, T.; Gao, D.; Ma, B.; Huang, L.; Xu, Z.; Lian, J. Biosynthesis of catharanthine in engineered *Pichia pastoris*. *Nat. Synth.* **2023**, *2*, 231−242.
(49) Bae, H.; Coller, J. Codon optimality-mediated mRNA degradation: Linking translational elongation to mRNA stability. *Mol. Cell* **2022**, *82* (8), 1467−1476.
(50) Zhang, L.; Hashimoto, T.; Qin, B.; Hashimoto, J.; Kozone, I.; Kawahara, T.; Okada, M.; Awakawa, T.; Ito, T.; Asakawa, Y.; Ueki, M.; Takahashi, S.; Osada, H.; Wakimoto, T.; Ikeda, H.; Ya, K. S.; Abe, I. Characterization of giant modular PKSs provides insight into genetic mechanism for structural diversification of aminopolyol polyketides. *Angew. Chem., Int. Ed.* **2017**, *56* (7), 1740−1745.
(51) Zhang, J.; Hansen, L. G.; Gudich, O.; Viehrig, K.; Lassen, L. M. M.; Schrübbers, L.; Adhikari, K. B.; Rubaszka, P.; Alvarez, E. C.; Chen, L.; D'Ambrosio, V.; Lehka, B.; Haidar, A. K.; Nallapareddy, S.; Giannakou, K.; Laloux, M.; Arsovska, D.; Jørgensen, M. A. K.; Chan, L. J. G.; Kristensen, M.; Christensen, H. B.; Sudarsan, S.; Stander, E. A.; Baidoo, E.; Petzold, C. J.; Wulff, T.; O'Connor, S. E.; Courdavault, V.; Jensen, M. K.; Keasling, J. D. A microbial supply chain for production of the anti-cancer drug vinblastine. *Nature* **2022**, *609* (7926), 341−347.
(52) Nicastro, R.; Brohée, L.; Alba, J.; Nüchel, J.; Figlia, G.; Kipschull, S.; Gollwitzer, P.; Pozuelo, J. R.; Fernandes, S. A.; Lamprakis, A.; Vanni, S.; Teleman, A. A.; Virgilio, C. D.; Demetriades, C. Malonyl-CoA is a conserved endogenous ATP-competitive mTORC1 inhibitor. *Nat. Cell Biol.* **2023**, *25* (9), 1303−1318.
(53) Ngo, J.; Choi, D. W.; Stanley, I. A.; Stiles, L.; Molina, A. J. A.; Chen, P. H.; Lako, A.; Sung, I. C. H.; Goswami, R.; Kim, M. Y.; Miller, N.; Baghdasarian, S.; Vasquez, D. K.; Jones, A. E.; Roach, B.; Gutierrez, V.; Erion, K.; Divakaruni, A. S.; Liesa, M.; Danial, N. N.; Shirihai, O. S. Mitochondrial morphology controls fatty acid utilization by changing CPT1 sensitivity to malonyl-CoA. *EMBO J.* **2023**, *42* (11), No. e111901.
(54) Li, C.; Gao, M.; Zhu, W.; Wang, N.; Ma, X.; Wu, C.; Wang, Q. Recent advances in the separation and purification of lactic acid from fermentation broth. *Process Biochem.* **2021**, *104*, 142−151.

https://doi.org/10.1021/acssuschemeng.4c05975
ACS Sustainable Chem. Eng. 2025, 13, 778−790